Performance Study of optical Modulator based on electro-optic effect

V Palodiya, S K Raghuwanshi
Department of Electronics Engineering,
Indian School of Mines
Dhanbad, India
E-mail: vikrampalodiya@gmail.com

Abstract. In this paper, we have studied and derive performance parameter of highly integrated Lithium Niobate optical modulator. This is a chirp free modulator having low switching voltage and large bandwidth. For an external modulator in which travelling-wave electrodes length L imposed the modulating switching voltage, the product of V_π and L is fixed for a given electro optic material Lithium Niobate. We investigate to achieve a low V_π by both magnitude of the electro-optic coefficient for a wide variety of electro-optic materials. A Sellmeier equation for the extraordinary index of congruent lithium niobate is derived. For phase-matching, predictions are accurate for temperature between room temperature 250^0C and wavelength ranging from 0.4 to $5\mu m$. The Sellmeier equations predict more accurately refractive indices at long wavelengths. Theoretical result is confirmed by simulated results. We have analysed the various parameters such as switching voltage, device performance index, time constant, transmittance, cut-off frequency, 3-dB bandwidth, power absorption coefficient and transmission bit rate of Lithium Niobate optical Modulator based on electro-optic effect.

1. Introduction

$LiNbO_3$ Optical modulators (LNOM) widely used in optical networks like metropolitan area networks (MANs) [1]. LNOM are based on the modulation of the material refractive index of the electric field, induced by an applied input voltage. LNOM achieve high performance and high reliability. LNOM also look promising for next-generation systems, because these next-generation systems require that optical modulators have almost zero chirp, X-cut LN modulators can be used with differential output drivers, by adjusting phases and amplitude of electrical signals precisely [2,3]. Due to the easier technology and the need of piezoelectrically induced static charge problems, X-cut modulators have been the initial choice for high speed broadband communication [4, 5]. In Fig 1 shows a few solutions to the interaction region, implemented through coplanar RF distributed electrodes. For an unbuffered X-cut modulator which, due to large velocity mismatch between the RF and optical modes, has a better modulation bandwidth than the lumped modulator but cannot achieve 10 Gbps operation. Reduction of the velocity mismatch is possible through the use of a low-permittivity dielectric buffer (silicon oxide, but also polymers has been exploited to this end) and of metal electrodes thickened through electroplating. X-cut modulators can very well cover 10 Gbps applications and are able to reach the 40 Gbps goal with modulation voltages of the order of 2 V in X-cut configurations. In LN-based modulator the use of junctions allows enhancement of the applied field in the active region. Reducing the switching voltage is important in high-speed operation, since it makes the design of the driver stage less critical. A commonly cited Sellmeier equation for congruent lithium niobate is based on refractive-index measurements at room temperature for wavelengths ranging from 404.6 nm to 3.39 mm [6,7] Since electric-field-poled LN was first demonstrated [8], interest in using periodically poled lithium niobate (PPLN) for optical applications has been growing steadily. This material offers a wide range of phase-matching possibilities [9] and high nonlinearities. This is not surprising since the data used to derive the Sellmeier equation do not extend beyond 3.39 mm. As discussed the multiphonon absorption in oxide materials leads to an exponential increase in absorption at wavelengths near the IR cutoff of the transparency range. For LN, the absorption coefficient at the temperature increases, the absorption edge moves toward shorter wavelengths and therefore has an even greater effect on the refractive index

in the mid-IR spectral region [10]. The potential applications for trace-gas sensing and countermeasures using mid-IR light generation in PPLN justify a revision of the Sellmeier equations to predict more accurately refractive indices at long wavelengths.

2. Theory of Lithium Niobate

$LiNbO_3$ modulator is used to get the highest electro-optic coefficient. Where (E_z), the externally applied electric field should be parallel to the X-axis shown in Fig.1. Therefore, in order to optimize the interaction between the electric field and the optical mode, in an X-cut wafer the electrodes should be located on both sides of the branches.

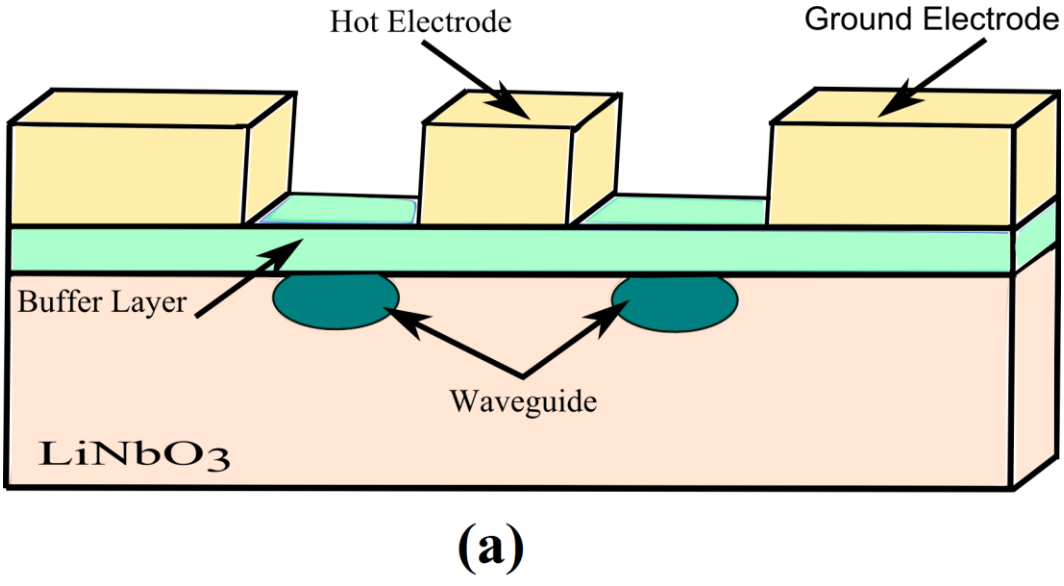

(a)

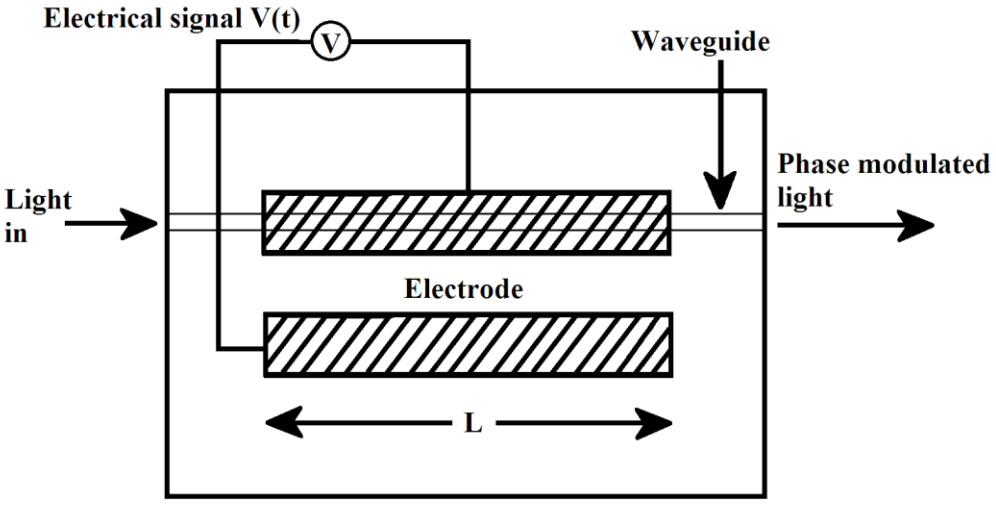

(b)

Figure 1(a) shows X-cut $LiNbO_3$ Phase Modulator and fig 1(b) Internal structure of $LiNbO_3$ Phase Modulator.

In these conditions, the extraordinary refractive-index change by electro-optic effect in $LiNbO_3$. In LN crystal symmetry, most of the electro-optic coefficients (r) in the matrix are zero, some of the electro-optic coefficients acquire equal values. However, the non-zero elements can be represented using the eq. (2.1)

$$\begin{cases} r_{13} = r_{23} = 9 \ \text{pm/V} \\ r_{33} = r_{51} = r_{42} = 30\text{pm/V} \\ r_{22} = -r_{12} = -r_{61} = 6.6 \ \text{pm/V} \end{cases} \quad (2.1)$$

However, the externally applied field will change all the components of the permittivity matrix. We confine the analysis for the case relevant to an application, and assumption, that the applied field is directed along the optical axis, i.e., that $\varepsilon_z = \varepsilon_3 \neq 0$ while both $\varepsilon_x = \varepsilon_1 = 0$ and $\varepsilon_y = \varepsilon_2 = 0$. In this case, considering only the nonzero element of *r* yield (for clarity, we partly revert to the expanded index notation in rectangular coordinates):

$$\Delta n_{xx} = \Delta n_{yy} = \Delta n_0 = -\frac{n_0{}^3 r_{13} \varepsilon_z}{2} \quad (2.2)$$

$$\Delta n_{zz} = \Delta n_e = -\frac{n_e{}^3 r_{33} \varepsilon_z}{2} \quad (2.3)$$

$$\Delta n_{yz} = \Delta n_{xz} = \Delta n_{xy} = 0 \quad (2.4)$$

Based on the proposed choice of the applied electric field, the off-diagonal elements of the permittivity matrix are always zero, and the principal axes remains unchanged with respect to the zero-field case. Moreover, the largest element r_{33} is exploiting, leading to a variation of the extraordinary index Δn_e, but the ordinary index Δn_0 experiences smaller variation in the X-cut configuration [11,12]. It is clear that; optical axis is parallel to the crystal surface and orthogonal to the waveguide axis. The waveguide axis runs along the *x* or *y*, while the crystal surface is an orthogonal to*y* or *x*, respectively. The optical mode polarization is transverse electric and it is apparent that, the electric field polarization is again along the optical axis, more specifically, it is horizontal. In such type of conditions, the modal RI is $n_{TE} = n_e$. Application of an electric field, along the *z* axis, which is parallel to the optical field and to the crystal surface leads to a variation of the modal RI:

$$\Delta n_{TE} = \Delta n_e = \frac{n_e{}^3 r_{33} E_Z}{2} \quad (2.5)$$

where n_e is the effective refractive index of the material based electro-optic modulator device, r_{33} is the corresponding electro-optic coefficient in pm/Volt, E_z is the integrated Mach-Zehnder intensity modulator. The theoretical value of the half-wave voltage of the integrated electro-optic modulator or switching voltage can be calculated using the expression

$$V_\pi = \frac{\lambda g}{L_m n_e^3 r_{33} \Gamma} \quad (2.6)$$

where λ is the operating signal wavelength in μm, g is the gap between electrodes in μm, L_m is the modulator length in cm, and Γ is confinement factor. The transmittance of an optical signal through the modulator using the following equation:

$$T_m = e^{-\alpha L_m} \quad (2.7)$$

where α is the power absorption coefficient in dB/cm. The resistance of modulator device can be measured by estimating the device dimensions as the following equation:

$$R = \rho \frac{L_m}{wd} \tag{2.8}$$

where ρ is the resistivity, w is the modulator width and d is the modulator thickness. The time constant of the modulator device τ.

$$\tau = RC \tag{2.9}$$

The cut-off frequency of the modulator device is calculated from the RC time constant as the following:

$$f_{cut-off} = \frac{1}{2\pi RC} \tag{2.10}$$

The relative refractive index change induces in an optical phase modulation is written as:

$$\Delta\emptyset = k_0 L_m \Delta n_e \tag{2.11}$$

where k_0=2π/λ is the wave number. The electrical 3-dB bandwidth f_{3-dB} for which modulation voltage V_m is reduced by $(1/\sqrt{2})$.

$$f_{3-dB} = \frac{1}{\pi R \varepsilon_{eff} C L_m} \tag{2.12}$$

where C is the capacitance in pF, ε_{eff} is the effective RF relative dielectric constant.

The electro-optic device reduces the bandwidth. Under the perfect velocity matching condition achievable modulation bandwidth f_m is:

$$f_m = \frac{6.84}{\alpha L_m} \tag{2.13}$$

For $LiNbO_3$ material, the investigation of both the thermal and spectral variations of the effective waveguide refractive-index (n_e) require empirical equation. The set of parameters required to completely characterize the temperature dependence of the refractive-index is given by, Sellmeier equation;

$$n_e = \sqrt{A_1 + A_2 H + \frac{A_3 + A_4 H}{\lambda^2 - (A_5 + A_6 H)^2} + \frac{A_7 + A_8 H}{\lambda^2 - A_9^2} - A_{10}\lambda} \tag{2.14}$$

where λ is the optical signal wavelength in μm and $H = T^2 - T_0^2$, T is the ambient temperature in K, and T_0 is the room temperature (300 K). The set of parameters of equation coefficients ($LiNbO_3$) are recast and dimensionally adjusted as: A_1= 5.35583, $A_2 = 4.629 \times 10^{-7}$, A_3= 0.100473,

$A_4 = 3.862 \times 10^{-8}$, A_5=0.20692, $A_6 = -0.89 \times 10^{-8}$, A_7= 100, $A_8 = 2.657 \times 10^{-5}$, A_9 = 11.34927, and A_{10}= 0.01533. Equation (1.10) can be simplified as the following:

$$n_e = \sqrt{A_{12} + \frac{A_{34}}{\lambda^2 - A_{56}^2} + \frac{A_{78}}{\lambda^2 - A_9^2} - A_{10}\lambda} \tag{2.15}$$

where: $A_{12} = A_1 + A_2 H$, $A_{34} = A_3 + A_4 H$, $A_{56} = A_5 + A_6 H$ and $A_{78} = A_7 + A_8 H$. Then the first and second differentiation of Equation (1.11) with respect to operating signals wavelength λ, which gives:

$$\frac{dn_e}{d\lambda} = \left(\frac{-\lambda}{n_e}\right)\left(\frac{A_{34}}{(\lambda^2 - A_{56}^2)^2} + \frac{A_{78}}{(\lambda^2 - A_9^2)^2} - A_{10}\right) \tag{2.16}$$

$$\frac{d^2 n_e}{d\lambda^2} = \left(\frac{1}{n_e}\right)\left(\frac{A_{34}\left(2 - (\lambda^2 - A_{56}^2)\right)}{(\lambda^2 - A_{56}^2)^2} + \frac{A_{78}\left(2 - (\lambda^2 - A_9^2)\right)}{(\lambda^2 - A_9^2)^2} - A_{10}\right) \tag{2.17}$$

The material dispersion based electro-optic modulator, D_{mat} which is given by the following equation:

$$D_{mat} = -\left(\frac{L_m(\Delta\lambda)\lambda}{c}\right)\left(\frac{d^2 n_e}{d\lambda^2}\right) \tag{2.18}$$

The modal-dispersion delay, D_{modal} for a multi-mode step-index electro-optic device with length L_m, is given by:

$$D_{modal} = \frac{L_m n_e \Delta n_e}{c} \tag{2.20}$$

Where the total dispersion coefficient, $D_t = D_{mat} + D_{modal}$. In addition to providing sufficient power to the receiver, the system must also satisfy the bandwidth requirements imposed by the rate at which data are transmitted. A convenient method of accounting for the bandwidth is to combine the rise times of the various system components and compare the result with the rise time needed for the given data rate and pulse coding scheme. The system rise time is given in terms of the data rate for non-return to zero pulse code by:

$$B_R(\mathrm{NRZ}) = \frac{0.7}{D_t} \tag{2.21}$$

In the same way, the device performance index (DPI) can be expressed as the following expression:

$$\mathrm{DPI} = \frac{f_m}{V_\pi} \tag{2.22}$$

3. Results and Discussion

We have investigated the recent progress of $LiNbO_3$ based electro-optic modulator device in high-speed photonic networks over a wide range of the affecting operating parameters. Based on the model equations analysis, set of the operating parameters as shown in Table 1.

Table 1. Proposed operating parameters for z–cut modulator device

Operating Parameter	Symbol	Value
Operating signal wavelength	λ	1.3 μm-1.55 μm
Spectral line width of the optical source	$\Delta\lambda$	0.1 nm
Ambient temperature	T	300 K$\leq$ T $\leq$ 320 K
Room temperature	T_0	300 K
Relative refractive-index change	Δn_e	0.05$\leq \Delta n \leq$0.09
Modulator length	L_m	5 cm$\leq L_m \leq$10 cm
Modulator width	W	2 cm$\leq$ w $\leq$5 cm
Modulator thickness	D	0.2 cm$\leq$ d $\leq$1 cm
Speed of light	C	3×10^{10}cm/sec
Gap between electrodes	G	0.1-0.35 μm
Electro-optic coefficient	r_{33}	30.8×10^{-10} cm/Volt
Applied electric field	E	2Volt/cm
Resistivity	ρ	$2.66\times 10^{-3}\Omega$cm
Confinement factor	Γ	0.8-0.95
Modulator device capacitance	C	0.2-0.4 pF
Effective RF relative dielectric constant	ε_{ff}	17.85
Power absorption coefficient	α	0.1-0.4 dB/cm

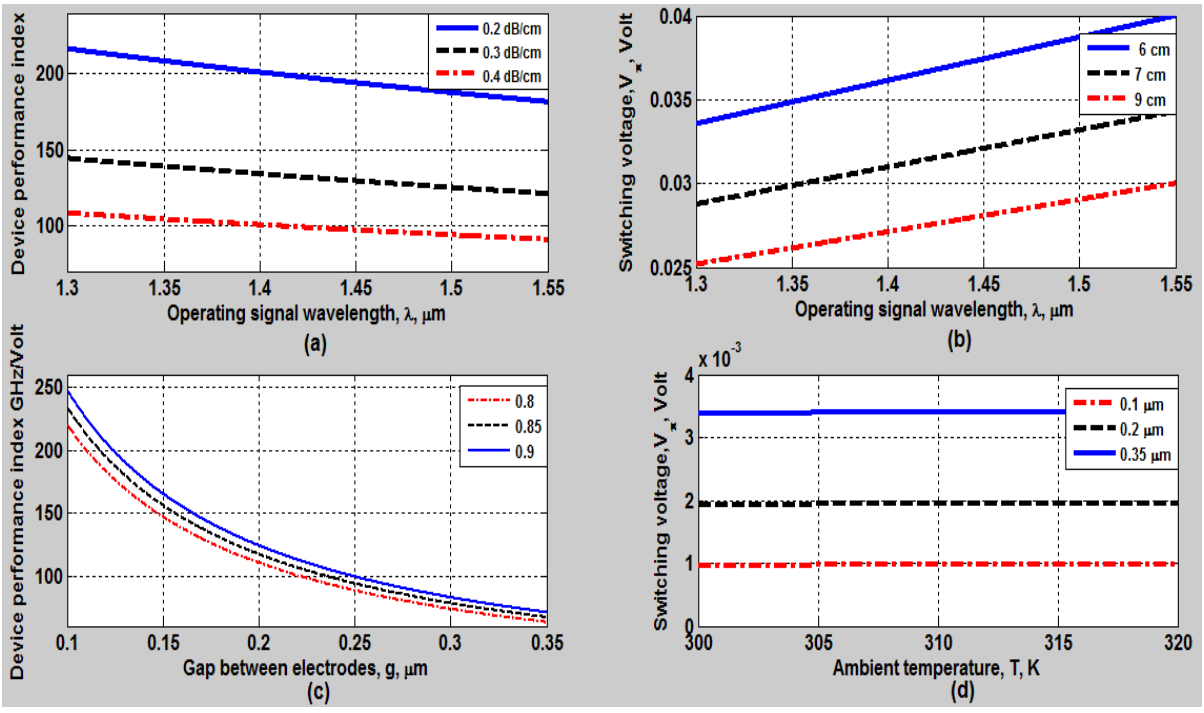

Figure 2: (a) Variations of the device performance index versus operating signal wavelength at the assumed set of parameters, (b) Variations of the switching voltage versus operating signal wavelength at the assumed set of parameters, (c) Variations of the device performance index against the gap between electrodes at the assumed set of parameters, (d) Variations of the switching voltage against ambient temperature at the assumed set of parameters.

Calculated results for λ as a function of DPI are plotted in Fig. 2 (a) for three values of power absorption coefficient α. This plot shows the operating optical signal wavelength increases, this leads to decrease in device performance index of the constant power absorption coefficient. As well, as power absorption coefficient increases, this results in decreasing of device performance at constant operating optical signal wavelength. In Fig. 2 (b) the operating optical signal wavelength increases, this leads to increase in switching voltage at constant modulator length. As well as modulator length increases, this results in decreasing of switching voltage at constant operating optical signal wavelength. Fig. 2 (c) has shown that as the gap between the electrodes increases, this leads to decrease in device performance index at constant confinement factor. As well as confinement factor increases, this result shows increasing of the device performance index at constant gap between electrodes. In Fig. 2 (d) has indicated that as ambient temperature increases, this leads slightly decrease in switching voltage at the gap between electrodes. As well as the gap between the electrodes increases, this result of increasing of switching voltage at constant ambient temperature.

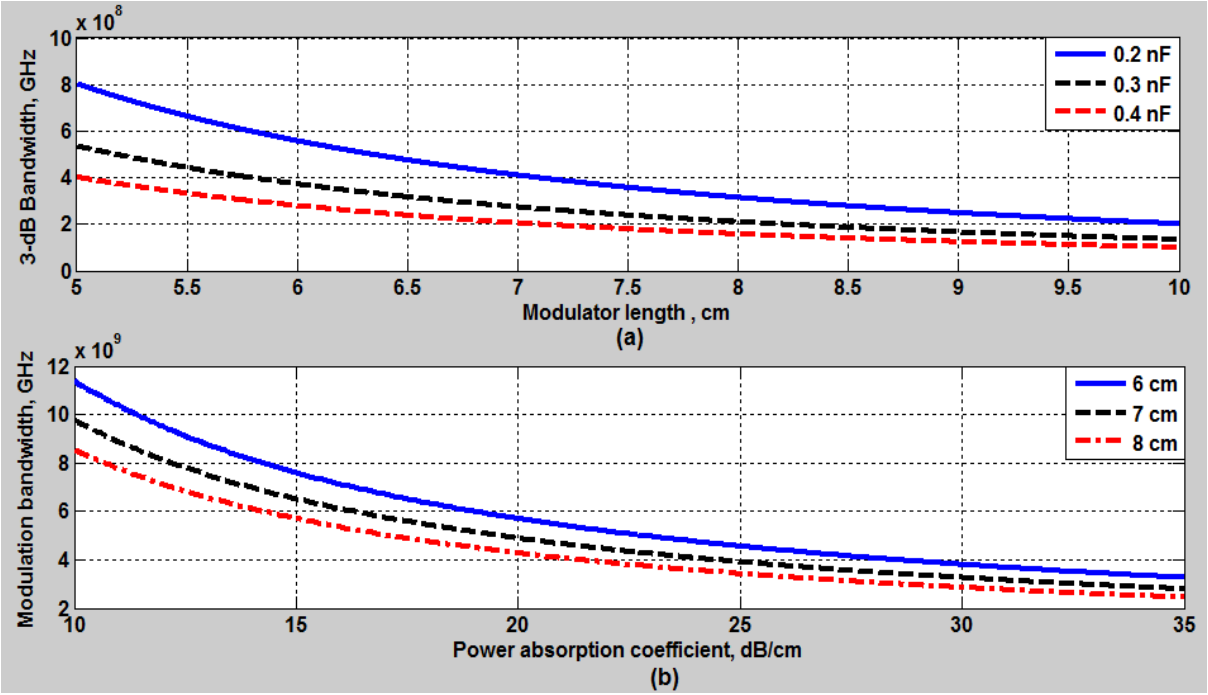

Figure 3: (a) Variations of 3-dB bandwidth against modulator length at the assumed set of parameters, (b) Variations of modulation bandwidth against power absorption coefficient at the assumed set of parameters.

As shown in Fig. 3 (a) has indicated that both modulator length and modulators capacitance increase, this results in decreasing of 3-dB bandwidth. In Fig. 3 (b) has shown that as both modulator length and power absorption coefficient increase, this leads to decrease of modulation bandwidth.

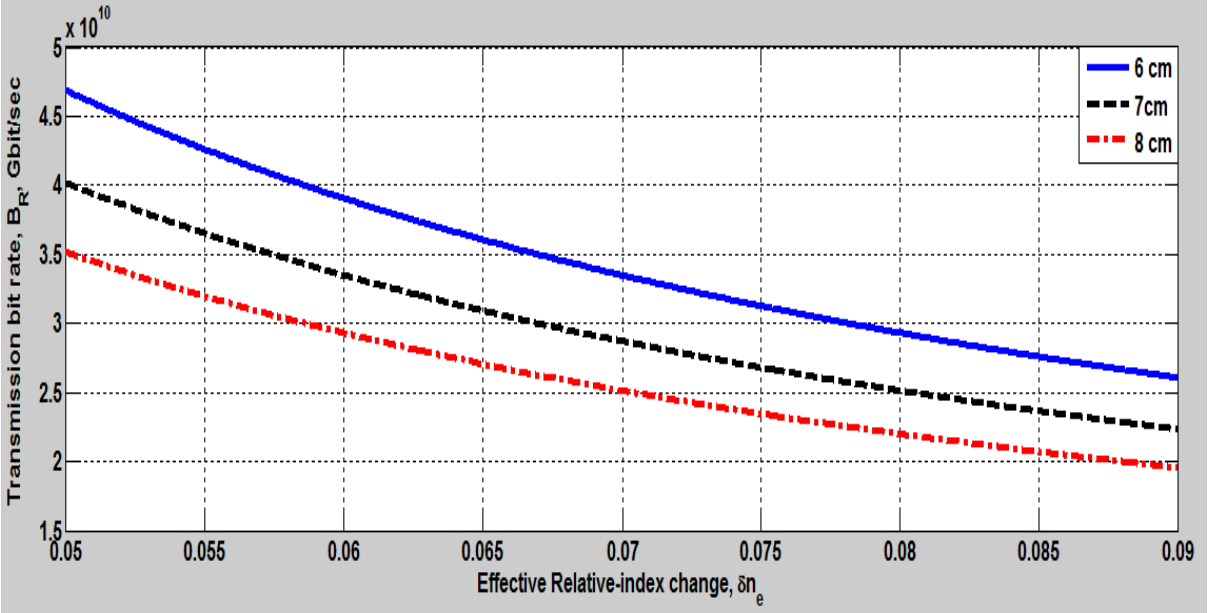

Figure 4: Variations of transmission bit rate versus effective refractive index of the assumed set of parameters.

In Fig. 4 shows that as effective relative refractive-index change and modulator length increases, these effects in decreasing in transmission bit rates of modulator devices.

4. Conclusion

We have investigated the control of light wave amplitude, phase and frequency using high speed lithium niobate optical modulation techniques. Optical MZ intensity modulators based on phase modulation can provide precise and agile control of light waves. In short, we deeply investigated the $LiNbO_3$ based electro-optic devices using a Sellmeier equation to handle the modulation bandwidth, switching voltage, cut-off frequency, transmission date rate and transmission bit rate length product. The optical modulator device performance parameters have been described and it is evident that the variation of these parameters leads to increase in the modulator device performance index.

5. References

[1]. Kawanishi T, Sakamoto T, and Izutsu M, 2007 *IEEE Journal of Selected Topics in Quantum Electronics* **13** 79–91.
[2]. Gheorma I, Savi P and Osgood Jr R, 2000 *IEEE Photon. Technol. Lett.* **12** 1618–1620.
[3]. Nagata H, 2000 *IEEE Photon. Technol. Lett.* **12** 1477–1479.
[4]. Shimotsu S, *et al.* 1995 *IEICE Trans. Commun.* 25–30.
[5]. Hu H, Ricken R, Sohler W and Wehrspohn R 2007 *IEEE Photonics Tech. Lett.* **19** 417-419.
[6]. Jundt H, Optics Lett. **22** 1553-1557.
[7]. Fieberg S, Streit L, Kiessling J, Becker P, 2012 Proc. SPIE 8240. doi: 10.1117/12.923571.
[8]. Wooten E L, Bloomfield CT, Kissa K. M, Yi-Yan A, Murphy, E. J, 2002 *Selected Topics in Quantum Electronics*, **6** 69 - 82.
[9]. Pham H.V and Okamura Y, *Journal of Advances in Optoelectronics.* **8** 1-8.
[10]. Lindsay, I. D, Lee C. J, Adhimoolam B and Boller K. J, 2006 Optics Express **14** 25-29.
[11]. Kondo J, Aoki K, kondo A, Eiiri T, 2005 *IEEE Photon. Tech. Lett.*, **17** 2077–2079.
[12]. Kawanishi T, Oikawa S, Higuma K, Matsuo Y and Izutsu M, 2001 *Electron. Lett.*, **37** 1244–1246.